IEEE Open Journal of the
Industrial Electronics Society

Received 14 May 2022; revised 9 June 2022; accepted 10 June 2022. Date of publication 14 June 2022;
date of current version 23 June 2022. The review of this paper was arranged by Associate Editor Fei Gao.

Digital Object Identifier 10.1109/OJIES.2022.3182977

An Integrated Topology of Three-Port DC-DC Converter for PV-Battery Power Systems

MOSTAFA I. MAREI [1] (Senior Member, IEEE), BADER N. ALAJMI [2] (Member, IEEE), IBRAHIM ABDELSALAM [3] (Senior Member, IEEE), AND NABIL A. AHMED [2] (Senior Member, IEEE)

[1]Electrical Power and Machines Department, Faculty of Engineering, Ain Shams University, Cairo 11517, Egypt
[2]Department of Electrical Engineering, College of Technological Studies, Public Authority for Applied Education and Training, Shuwaikh 70654, Kuwait
[3]Electrical and Control Department, College of Engineering & Technology, Arab Academy for Science, Technology & Maritime Transport, Cairo 2033, Egypt

CORRESPONDING AUTHOR: IBRAHIM ABDELSALAM (email: i.abdelsalam@aast.edu)

This work was supported in part by the Public Authority for Applied Education and Training (PAAET), and in part by PAAET and the College Of Technological Studies under Project TS-21-09.

ABSTRACT This paper introduces an integrated topology of isolated three-port dc-dc converter (TPC) to interface Photovoltaic (PV) and battery for standalone system. To guarantee zero circulating current flow between different ports while permitting bidirectional power flow at the battery port, auxiliary switches are utilized with the active bridges of the proposed TPC topology. In addition, a simple switching scheme based on Pulse Width Modulation (PWM) is proposed for the input ports of the TPC. This action eliminates the need for the phase shift modulation used for conventional isolated TPCs. While the PV port is controlled to track the maximum power point, the battery port is managed to regulate the load voltage. The paper presents the detailed mathematical analysis of the different operation modes of the proposed integrated TPC topology and the estimated control limits during charging and discharging of the battery. Consequently, dynamic limiters for the duty cycle of each port are set. The proposed integrated TPC based PV-battery system is simulated using PSCAD/EMTDC software package to validate the analysis of different operation modes and to assess the dynamic performance of the system. Moreover, experimental results are presented to authenticate different operation modes of the proposed TPC topology and to evaluate the dynamic behavior of the integrated PV-battery system.

INDEX TERMS Three-port dc-dc converter, PV-battery power system, voltage regulation.

I. INTRODUCTION

Recently, there is a remarkable growth in using isolated Photovoltaic (PV) systems as a distributed generator (DG). The use of Energy Storage Systems (ESS) in conjunction with PV modules is mandatory to overcome the intermittent nature of PV systems feeding isolated loads. Among different ESS, batteries are used widely for stand-alone PV systems to balance the harvested PV power and load requirement. To accommodate diverse operating voltage levels of PV module, battery, and load, either two independent dc-dc converters or integrated three-port converters (TPC) are used. The compactness and reduced components count and weight are the main advantages of the TPC over the independent dc-dc converters [1], [2]. The TPC topologies can be categorized into nonisolated [3]–[5], partially-isolated [6]–[9], and fully-isolated topologies [10]–[13].

The fully-isolated TPCs are based on a high frequency transformer which is not only offering galvanic isolation between different ports, but allows achieving high voltage gain and eliminates leakage currents [14]. Many topologies fully-isolated TPCs are presented in literature. A topology based on center-taped multiport transformer is presented in [15]. Beside the complexity and the large components count are the main disadvantages of this topology. Many TPCs are developed using three active half or full bridges (TAB) where phase shift angles between different bridges are controlled to set the power transfer between ports [16]–[21]. As the leakage inductances of the transformer are small, external inductances

are added to achieve proper control range of phase shift angles that satisfy the required power flow between ports [22]. In addition to the unavoidable impact of using external inductors on the performance of the TAB, sophisticated control techniques are required to reduce circulating currents between the ports [23]. A topology for isolated TPC based on dual high-frequency transformer to interface two dc sources and a load is presented [24]. The main advantage of this topology is the reduction of circulating currents between ports compared with the TAB based on three-winding transformer. However, it comes on the account of increased components count and size of the TPC. The authors presented a unidirectional multiport dc/dc converter based on a two-quadrant inverter topology for interfacing PV systems [25]. This topology eliminates the circulating currents between ports. However, it is not suitable for integrating ESS for stand-alone applications.

This paper presents a novel TPC topology for integrated PV–battery system to feed an isolated load. The contributions of this paper are summarized as follows. The proposed TPC topology is based on auxiliary switches to guarantee zero circulating current flow between different ports while permitting bidirectional power flow at the battery port. Moreover, a new and simple switching scheme is presented for the proposed TPC to avoid the aforementioned associated problems of the phase shift modulation used for conventional isolated TPCs. As a result, there is no need to add external inductors which in one of the advantages of the proposed system. This action renders the proposed TPC topology to outperform the existing TAB. Furthermore, different operation modes of the proposed converter are analyzed and limits of the controlled variables are derived. The paper is organized as follows. Section II introduces the proposed TPC for integrating PV and battery to feed an isolated load. The detailed analysis of the operation modes during battery charging and discharging are presented in Sections III and IV, respectively. Section V provides simulation results and the experimental evaluation of the proposed system is demonstrated in Section VI. Finally, the paper is concluded in Section VII.

II. PROPOSED TOPOLOGY OF THE THREE-PORT CONVERTER

Fig. 1 shows the proposed PV interfacing system which is based on an isolated three-port dc/dc converter. The proposed TPC is centered on a high-frequency transformer. The PV and the battery pack are connected to separate winding of the high-frequency transformer through individual H-bridge inverters. The load is connected through a rectifier to the output winding. The number of turns of the PV, battery pack, and load ports windings are $N_{pv} : N_b : N_o$. The PV module is connected to its H-bridge through a diode D_{pv} to prevent circulating current from the battery port and to guarantee unidirectional power flow from the PV port. In contrast, the battery pack is connected to an H-bridge through a bidirectional switch (S_f, S_r) to guarantee zero circulating current with the PV port converter during the discharging operation and to control the charging process.

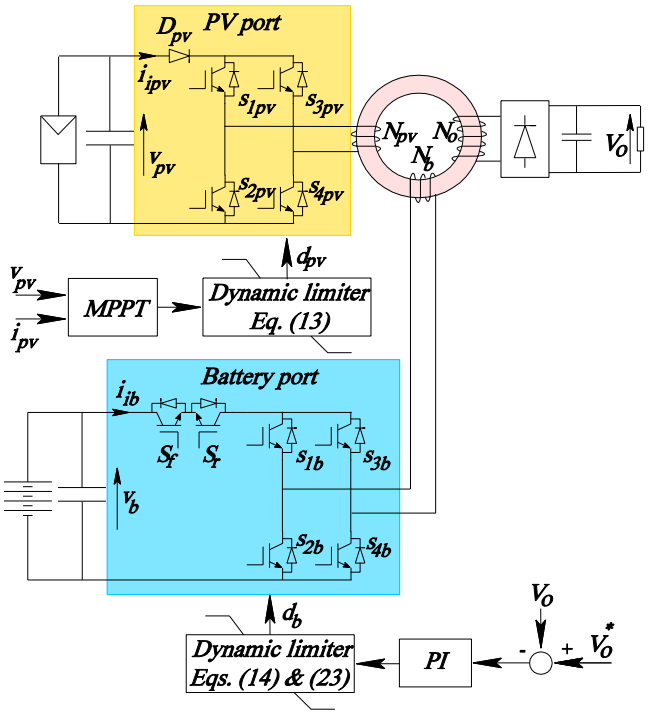

FIGURE 1. The proposed TPC for integrated PV-battery system.

Fig. 2 illustrates two circulating current paths in classical TPC when H-bridges are operated at positive states, S_{1pv} , S_{4pv} S_{1b} , and S_{4b} are turned-on. When the PV terminal voltage is lower than the referred voltage of the battery pack, $v_{pv} < \acute{v}_b$, the current circulates between the battery pack and the capacitor connected to the PV module through the S_{1b}, D_{1pv}, D_{4pv}, and S_{4b}, as demonstrated in Fig. 2(a). The circulating current is only limited by the leakage inductances of the PV and battery ports windings, L_{pv} and L_b, respectively. Another circulating current path is shown in Fig. 2(b) when $v_{pv} < \acute{v}_b$. In TPC controlled by phase shift techniques, external inductors are added to the ports to obtain required range of angle control which reduce the circulating current. However, the power electronics switches and magnetic components should be overrated to withstand circulating currents between ports. The proposed TPC topology eliminates circulating current flow between different ports and hence no need for either external inductor or the sophisticated phase angle shift controllers.

As illustrated in Fig. 1, the control objectives of the proposed system are to track the maximum power point of the PV module and regulating the output load voltage without circulating current between PV and battery ports. The PV port is controlled using Maximum Power Point Tracking (MPPT) to harvest the maximum power from the PV module and deliver it to the load. The Perturb and Observe (P&O) based MPPT technique is used to modulate the duty cycle of the PV port inverter, d_{PV} [26], [27]. The battery port is controlled to regulate the load voltage at the desired level regardless the status of the PV module. A simple PI controller is used

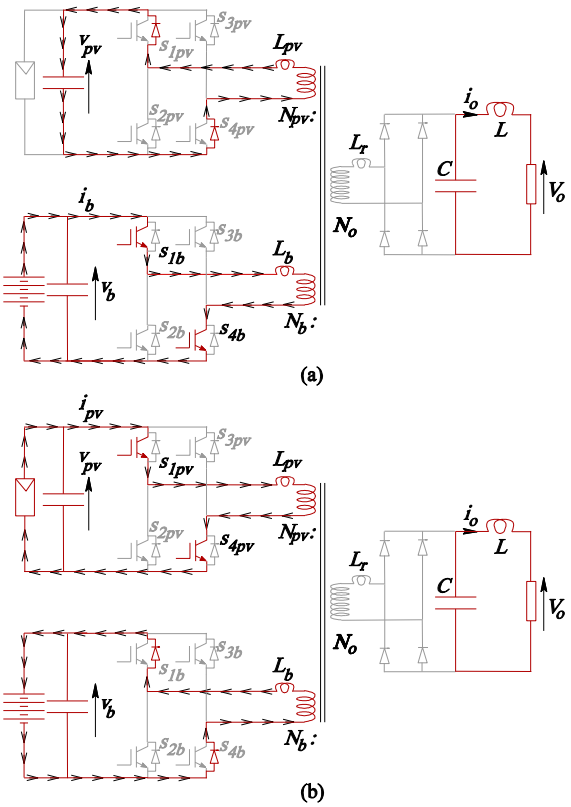

FIGURE 2. Circulating current in conventional TPC: (a) $v_{pv} < v'_b$ and (b) $v_{pv} > v'_b$.

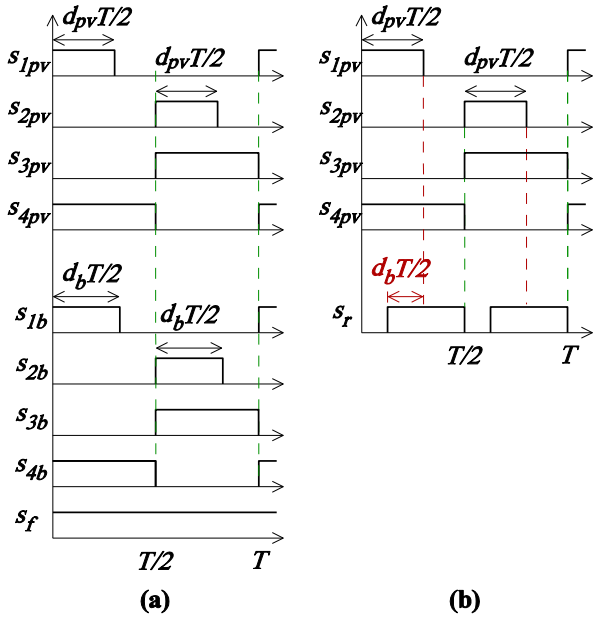

FIGURE 3. The switching scheme of the proposed TPC: (a) During battery discharging and (b) Battery charging.

to regulate the load voltage v_o by controlling the duty cycle of the battery port inverter, d_b. This action implies that the battery port is controlled to either support the deficiency of the harvested PV power or absorb the excess power extracted from the PV, due to the varying weather or loading conditions.

A simple switching technique is used for the H-bridges. For the H-bridge of the PV module, the switches of one leg, S_{3PV} and S_{4PV}, are complemented each half-cycle while the pulse width of other leg switches, S_{1PV} and S_{2PV}, are modulated according to d_{PV}, to control the power flow from the PV port. During discharging mode of operation, the same PWM switching scheme used for the PV inverter is applied for the battery port inverter, but with a duty cycle d_b, as illustrated in Fig. 3(a). In addition, the forward switch S_f is turned-on to enable power transfer from the battery port to the load, while the reverse switch S_r is turned-off to prevent formation of a path for circulating current that may flows from the PV port to the battery if $v_{pv} < v_b$. During the charging operation, the H-bridge of the battery port is disabled and S_f is turned-off while S_r is modulated using d_b, as shown in Fig. 3(b), to allow for reverse power flow. As a result, the battery port works as a buck converter fed from a body-diodes-rectifier. It is worth mentioned that d_b is measured from the falling edge of modulating signals of the PV port, S_{1PV} and S_{2PV}, where the PV port is enabled to charge the battery in addition to feeding the load. Moreover, the gating signal for S_r is extended to the end of half-cycle period to allow for discharging the stored energy in the leakage inductance of the winding into the battery.

The bidirectional power flow operation of the battery port is controlled by the sign of d_b. The PI controller is adjusted to generate positive values for d_b for discharging operation, forward power flow, and negative values for reverse power flow during charging operation.

III. OPERATION MODES DURING BATTERY CHARGING

There are many different modes of operations for the proposed TPC during battery charging and discharging. The five operations modes of the proposed converter, per positive half-cycle during battery charging, are shown in Fig. 4. The current and voltage waveforms of the transformer windings are traced in Fig. 5. Neglecting the windings resistances, the magnetizing current, and the voltage drop across switches, the converter model, referred to the winding of the PV port, can be written as:

$$L_{pv} di_{1pv}/dt = v_{1pv} - E \tag{1}$$

$$L'_b dl'_{1b}/dt = v'_{1b} - E \tag{2}$$

$$L'_r di'_r/dt = E - v'_r \tag{3}$$

$$i'_r = i_{1pv} + i'_{1b} \tag{4}$$

where the suffix $'$ indicates referring to the winding of the PV port, L_{pv}, $L'_b = (N_{pv}/N_b)^2 L_b$, and $L'_r = (N_{pv}/N_o)^2 L_r$ are the leakage inductances of the transformer windings connected to PV, battery, and output ports, respectively, i_{1pv}, $i'_{1b} = (N_b/N_{pv})i_{1b}$, and $i'_r = (N_o/N_{pv})i_r$ are the windings currents of PV, battery, and output ports, respectively, v_{1pv}, $v'_{1b} = (N_{pv}/N_b)v_{1b}$, and $v'_r = (N_{pv}/N_o)v_r$ are the windings voltages

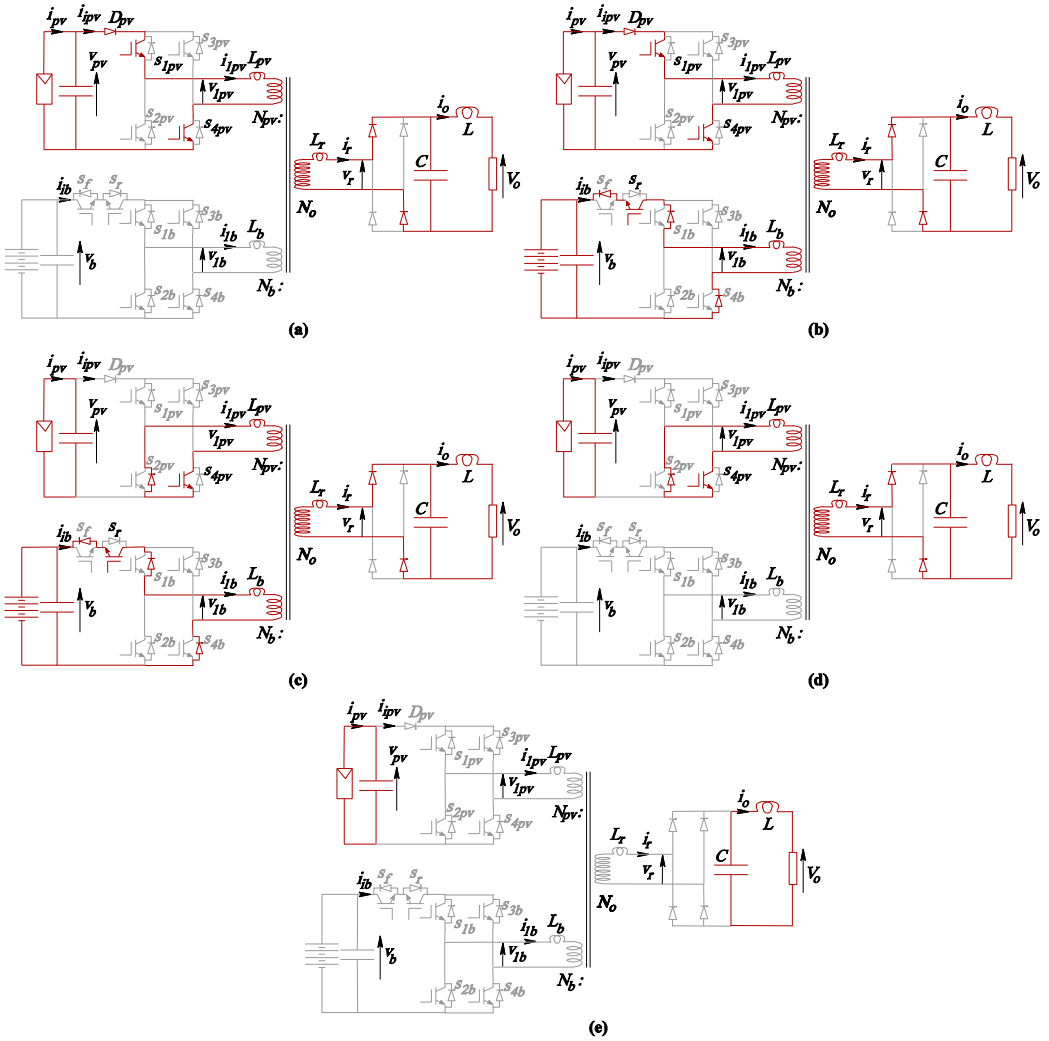

FIGURE 4. **The operation modes of the proposed TPC during battery charging.**

of PV, battery, and output ports, respectively, and E is the transformer induced voltage at the winding of the PV port. The following subsections present the analysis of different operating modes during battery charging operation.

A. MODE 1

This mode is initiated when the PV port inverter is turned-on, S_{1pv}=S_{4pv}=1, while the switches of the battery port are turned-off as illustrated in Fig. 4(a). During this mode, the harvested power from the PV is transferred to the load side through the rectifier. Accordingly, the PV port current is rising as shown in Fig. 5. Assuming successful output voltage regulation and substituting $i'_{1b} = 0$ and $v'_r = v'_o$ in (1), (3), and (4), the PV port current at the end of mode 1 is estimated from:

$$I_{pv1} = \frac{\alpha(d_{pv} - d_b)}{2fL_{pv}} \left(v_{pv} - v'_o\right) \tag{5}$$

where $\alpha = L_{pv}/L_{pv} + L'_r$, v_{pv} is the PV module voltage, and v'_o is the load voltage referred to the PV port.

B. MODE 2

When S_r is switched-on at t_1, Fig. 5, the battery starts to charge through the body-diodes of the battery port inverter as demonstrated in Fig. 4(b). During this mode, the battery and PV ports currents rise to their maximum values at t_2 when the PV port is switched to the zero state, S_{1pv}=0. The battery and PV ports currents, I_b and I_{pv2}, are calculated by solving (1) to (4) and using (5) as:

$$I_b = \frac{d_b N_{pv}}{2f\left(L'_b + \alpha L'_r\right) N_b} \left[(1-\alpha)\, v_{pv} + \alpha v'_o - v'_b\right] \tag{6}$$

$$I_{pv2} = \frac{\alpha}{2fL_{pv}} \left\{ d_{pv}(v_{pv} - v'_o) + \frac{d_b}{\alpha + L'_b/L'_r} \left[(1-\alpha)\, v_{pv} + \alpha v'_o - v'_b\right] \right\} \tag{7}$$

where v'_b is the battery pack voltage referred to the PV port.

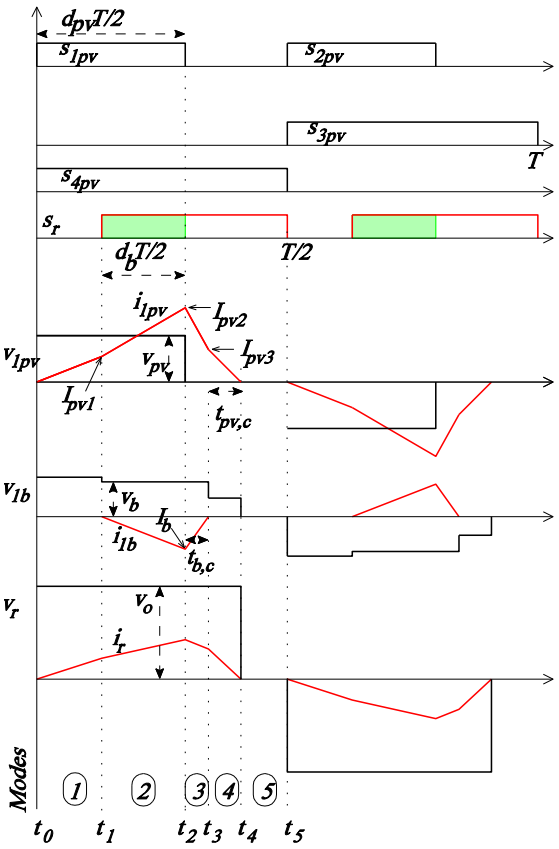

FIGURE 5. Transformer voltages and currents during battery charging.

The condition to establish the charging process is $E > v_b'$, which results in the following inequality,

$$N_b > \frac{V_b}{\left((1-\alpha)\,V_{pv}/N_{pv} + \alpha V_o/N_o\right)} \tag{8}$$

where V_b is the maximum battery voltage, V_{pv} is the PV module voltage at the maximum power point, and V_o is the nominal load voltage. The turn's ratio between windings of the PV and load ports is selected based of their voltage levels. Moreover, the number of turns of the battery pack port winding N_b is designed according to (8) to guarantee the charging operation.

C. MODE 3

Once the modulating leg of the PV port inverter is turned-off, Fig. 4(c), the stored energy in the leakage inductances of the transformer is freewheeling through S_{4pv} and the body-diode of S_{2pv} to charge the battery pack and to feed the output port. This mode continues until the leakage inductance of the battery port winding is completely discharged, i_{1b}=0, as indicated in Fig. 5. By using (6) and (7) as initial values for the battery and PV ports currents, respectively, and substituting v_{1pv}=0, (1) to (4) can be resolved to express the duration of mode 3, $t_{b,c}$, and the PV port current at t_3 as follows:

$$t_{b,c} = \frac{d_b}{2f}\left[\frac{(1-\alpha)\,v_{pv}}{v_b' - \alpha v_o'} - 1\right] \tag{9}$$

$$I_{pv3} = \frac{\alpha}{2fL_{pv}}\left[d_{pv}\left(v_{pv} - v_o'\right) + d_b\left(v_o' - \frac{(1-\alpha)\,v_{pv}v_o'}{v_b' - \alpha v_o'}\right)\right] \tag{10}$$

D. MODE 4

During this mode, the battery port becomes floating and the stored energy in L_{pv} and L_r continues to feed the output port through S_{4pv} and the body-diode of S_{2pv}, as indicated in Fig. 4(d). By solving (1), (3), and (4) using (10) as initial value of PV port current for mode 4, the duration of this mode is calculated form,

$$t_{pv,c} = \frac{1}{2f}\left[d_{pv}\left(\frac{v_{pv}}{v_o'} - 1\right) + d_b\left(1 - \frac{(1-\alpha)\,v_{pv}}{v_b' - \alpha v_o'}\right)\right] \tag{11}$$

According to (2), the floating voltage across battery port winding is dropped to E.

E. MODE 5

During this mode, the high-frequency transformer becomes de-energized as indicated in Fig. 4(e) where the windings voltages and currents are null. At the end of this mode, the negative half-cycle is initiated by turning-off S_{4pv} and S_r and turning-on S_{2pv} and S_{3pv}. Five modes of operation, similar to the positive half-cycle modes but with different operating switches, takes place.

Referring to Fig. 5, to keep the Discontinuous Current Mode (DCM), the following inequality should be satisfied

$$d_{pv}T/2 + t_{b,c} + t_{pv,c} < T/2 \tag{12}$$

Substituting (9) and (11) in (12), results in the following condition for DCM during battery pack charging,

$$d_{pv} < v_o'/v_{pv} \tag{13}$$

The dynamic limiter on d_{pv} is set according to (13), as shown in Fig. 1. Referring to Fig. 3(b), the lower limit on the duty cycle of the battery port is set according to

$$-d_{pv} < d_b \tag{14}$$

The extracted power form the PV module and the power transferred to the battery can be estimated by calculating the average currents of the PV module and battery pack, respectively, from Fig. 5 and using (5), (6), (7), and (9) as follows:

$$P_{pv} = \frac{\alpha\, v_{pv}}{4fL_{pv}}\left[d_{pv}^2(v_{pv} - v_o') + \frac{d_b^2}{\alpha + L_b'/L_r'}\left((1-\alpha)\,v_{pv} + \alpha v_o' - v_b'\right)\right] \tag{15}$$

$$P_b = \frac{(1-\alpha)\,d_b^2}{4f\left(L_b' + \alpha L_r'\right)}\left(\frac{(1-\alpha)\,v_{pv}}{v_b' - \alpha v_o'} - 1\right)v_{pv}v_b' \tag{16}$$

IV. OPERATION MODES DURING BATTERY DISCHARGING

During shading, the battery port shares the load power with the PV port. There are five operations modes of the proposed

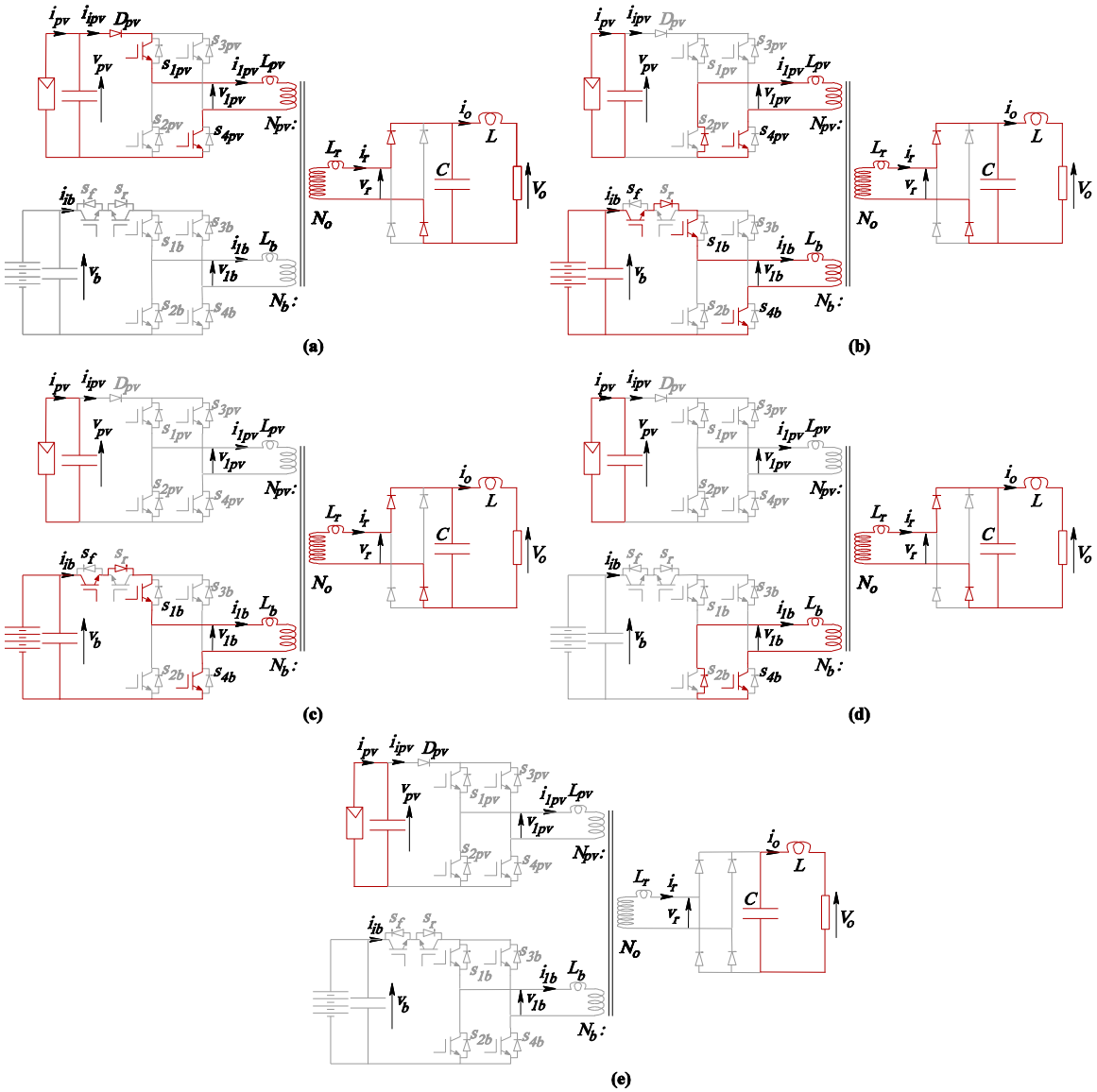

FIGURE 6. The operation modes of the proposed TPC during battery discharging.

converter per half-cycle during battery discharging as presented in Fig. 6. The current and voltage waveforms of the three ports windings are displayed in Fig. 7. The analysis of the proposed TPC during discharge operation is similar to a topology proposed by the authors based on two-quadrant inverters [25].

A. MODE 1

This mode is initiated when the inverters of the PV port and battery port are switched-on to the positive state, S_{1pv}=S_{4pv}= S_{1b} =S_{4b} =1, as illustrated in Fig. 6(a). In addition, S_f is turned-on to enable power transfer from the battery port to the load, while S_r is turned-off to insure zero circulating current between the PV and the battery ports. It is worth mentioned that (8) is derived from the condition $E > v'_b$ to establish the charging process. This action results in blocking the battery port during mode 1 of battery discharging. The PV port current is rising as shown in Fig. 7 and the harvested PV power is transferred to the load side. The peak value of the PV port current is calculated by substituting $i'_{1b} = 0$ and $v'_r = v'_o$ in (1), (3), and (4) as:

$$I_{pv} = \frac{\alpha d_{pv}}{2fL_{pv}} \left(v_{pv} - v'_o\right) \tag{17}$$

B. MODE 2

This mode is started when the PV port inverter is turned to the zero state. Consequently, the stored energy in the leakage inductance of the PV port winding is transferred to the load through S_{4pv}, the body diode of S_{2pv}, and the output rectifier, as indicated in Fig. 6(b). Simultaneously, the battery port current rises to feed the load side. Solving (1) to (4) and using

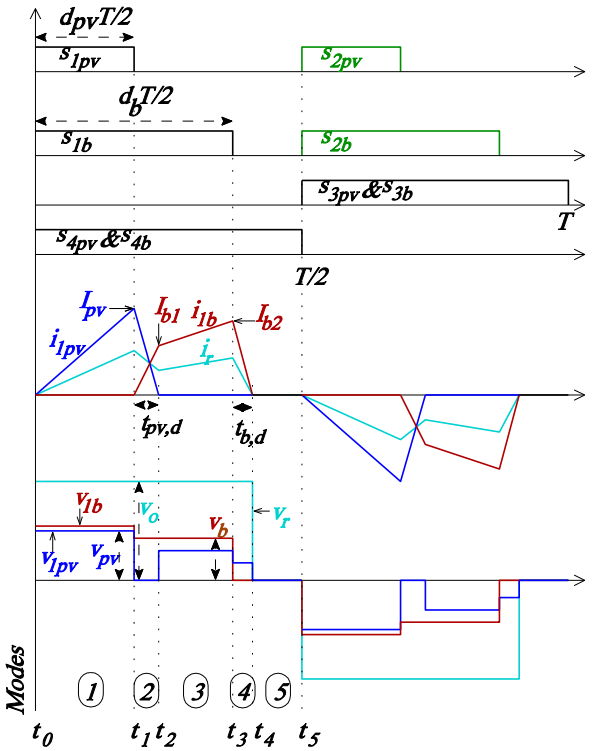

FIGURE 7. Transformer voltages and currents during battery discharging.

(17), the duration of this mode and the battery port current at the end of mode 2 are formulated as follows:

$$t_{pv,d} = \frac{\alpha d_{pv}}{2fL_{pv}} \left(v_{pv} - v'_o\right) \frac{L_{pv}L'_b + L_{pv}L'_r + L'_bL'_r}{L'_bv'_o + L'_rv'_b} \tag{18}$$

$$I_{b1} = \frac{\alpha d_{pv}N_{pv}}{2fL_{pv}N_b} \left(v_{pv} - v'_o\right) \frac{\left(L_{pv} + L'_r\right)v'_b - L_{pv}v'_o}{L'_bv'_o + L'_rv'_b} \tag{19}$$

C. MODE 3

During this mode, the battery is continuing to feed the output side until the battery port is switched to the zero state, as demonstrated in Fig. 6(c). Since the PV port is floating, $v_{1pv} = E$ which is less than v_{1b} due to the voltage drop across the leakage inductance L_b and the turns ratio N_{pv}/N_b which is less than unity. Resolving (2), (3), and (4) and substituting (18) and (19), the peak current of the battery port is given by:

$$I_{b2} = \frac{N_{pv}}{2f\left(L'_b + L'_r\right)N_b} \left\{d_{pv}\left[(1-\alpha)v_{pv} + \alpha v'_o - v'_b\right] + d_b\left(v'_b - v'_o\right)\right\} \tag{20}$$

D. MODE 4

At this mode, the battery port inverter is switched to the zero state and the stored energy in L_b is transferred to the load through S_{4b}, the body diode of S_{2b}, and the output rectifier, as indicated in Fig. 6(d). Resolving (2) to (4) and using (20), the duration of this mode is expressed as follows:

$$t_{b,d} = \frac{1}{2f}\left[(1-\alpha)\,d_{pv}\left(\frac{v_{pv}}{v'_o} - 1\right) + \left(d_b - d_{pv}\right)\left(\frac{v'_b}{v'_o} - 1\right)\right] \tag{21}$$

E. MODE 5

Similar to mode 5 of battery charging operation, the transformer becomes de-energized as indicated in Fig. 6(e). During the negative half-cycle, which is initiated after this mode, there are five modes of operation, similar to the positive half-cycle modes but with different operating switches.

Referring to Fig. 7, to keep the DCM, the following inequality should be satisfied

$$d_bT/2 + t_{b,d} < T/2 \tag{22}$$

Substituting (21) in (22), results in the following condition for DCM discharging operation of the battery pack,

$$d_b < d_{pv}\left(1 - (1-\alpha)\,v_{pv}/v'_b\right) + v'_o/v'_b\left(1 - \alpha d_{pv}\right) \tag{23}$$

Equations (14) and (23) set the lower and upper bounds of the dynamic limiter on d_b, respectively, as presented in Fig. 1. The harvested power from the PV module and the power fed from the battery pack are given by:

$$P_{pv} = \frac{\alpha d_{pv}^2}{4fL_{pv}} v_{pv}\left(v_{pv} - v'_o\right) \tag{24}$$

$$P_b = v_b\left[\frac{1}{2}\left(d_b - d_{pv}\right)\left(I_{b1} + I_{b2}\right) - I_{b2}f\,t_{pv,d}\right] \tag{25}$$

TABLE 1 System Parameters

PV module	300W, 54V @ STC
Battery voltage	48V
Rated power	300W
Load voltage, V_o	110V
Switching frequency	10 KHz
$N_{pv} : N_b : N_o$	10:13:33
Leakage inductance of PV winding, L_{pv}	6.51 μH
Leakage inductance of battery winding, L_b	9.6 μH (L_b' =6.67 μH)

V. SIMULATION RESULTS

The proposed TPC based PV-battery integrated system is simulated using EMTDC/PSCAD software to examine its dynamic performance. The system parameters are given in Table 1. According to (8), the number of turns of the battery port winding is selected to be 13 to allow for battery charging with the given parameters. The dynamic performance of the proposed PV-battery integrated system is evaluated under different disturbances at load and irradiance level. Fig. 8(a) and (b) show the load voltage and current, respectively. The load resistance is suddenly changed from 60Ω to 50Ω at $t = 0.2$s, to 46Ω at $t = 0.3$s, to 40Ω at $t = 0.4$s, and to 60Ω at $t = 0.7$s. In addition, the irradiance level is reduced from 1000 W/m^2 to 750 W/m^2 at $t = 0.5$s, to 500 W/m^2 at $t = 0.6$s, and to 250 W/m^2 at $t = 0.7$s, as indicated in Fig. 9(a). Fig. 8(c) indicates

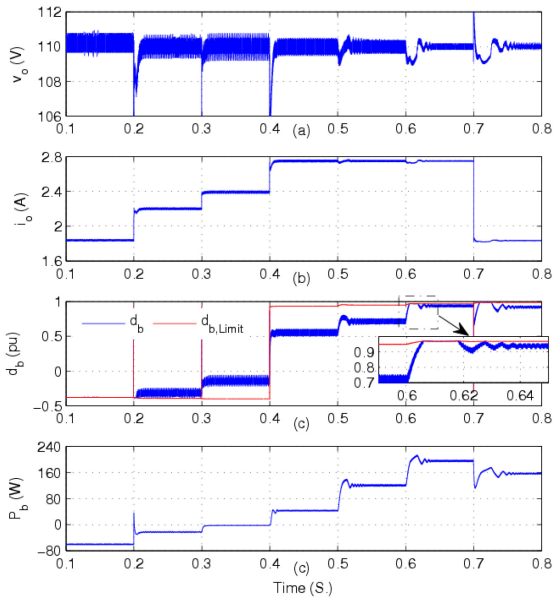

FIGURE 8. Dynamic performance of the battery port and the load-side.

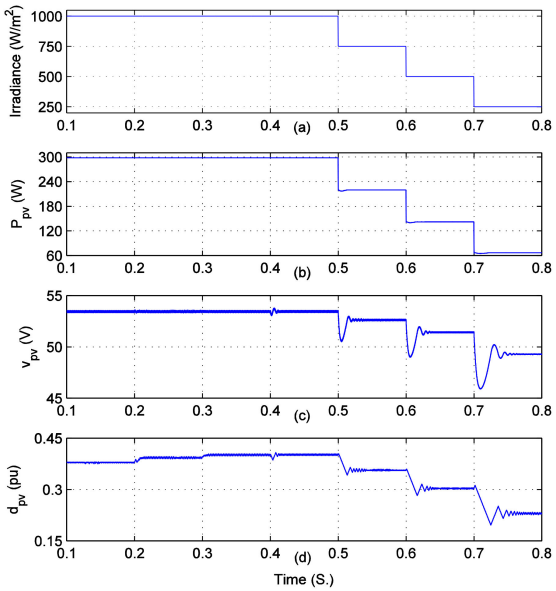

FIGURE 9. Dynamic performance of the PV port.

that the proposed system succeeds to control the duty cycle of the battery port to tightly regulate the load voltage at the set value, 110V, regardless load changes or irradiance variations. Consequently, the power fed from the battery pack, shown in Fig. 8(d), supplements the harvested power from PV module, Fig. 9(b). In addition, the power of the battery port is reversed smoothly at $t = 0.4$s, to keep the load voltage when the load power exceeds the harvested PV power. Fig. 9(c) shows the voltage of the PV module.

During the initial period of light load, $t<0.2s$, d_b is limited at the value of $-d_{pv}$, as given by (14) and indicated in Fig. 8(c). Moreover, when the irradiance is low and the load is rated,

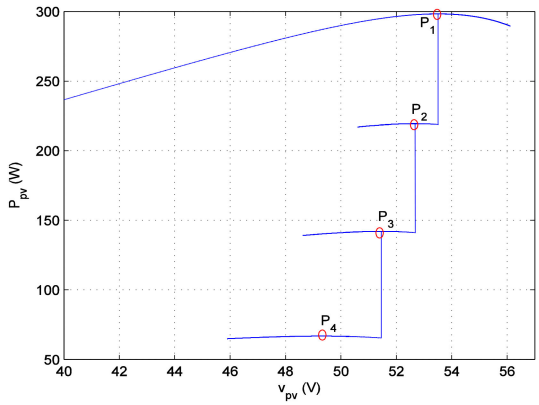

FIGURE 10. Power-Voltage trajectory of the PV module.

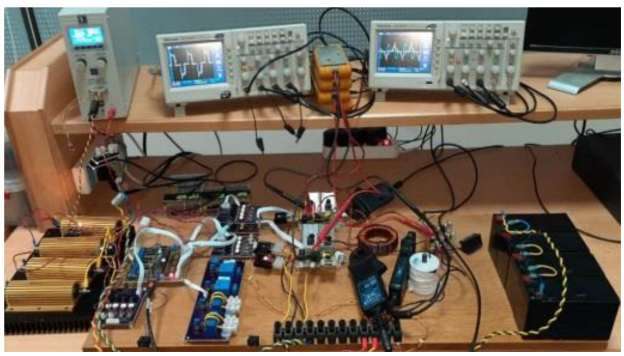

FIGURE 11. The experimental prototype.

$0.6 < t < 0.7$s, d_b is increased and hit its limit, given by (23), to transfer more power from the battery port to keep the load voltage as indicated in Fig. 8. Fig. 9(d) demonstrates that the MPPT unit is controlling d_{PV} to harvest the maximum power from the PV module under the hypothetical changes in irradiance level. It can be shown that d_{pv} is lower than its limit value, given by (13). The voltage-power trajectory of the PV module, shown in Fig. 10, indicates that the PV port successfully harvests and delivers the maximum power.

VI. EXPERIMENTAL RESULTS

Fig. 11 shows the laboratory prototype with the parameters given in Table 1. The programmable power supply (EA-PS-83600-10 with analogue interface) and the microcontroller (CY8C5888LTI-LP097) are utilized to emulate the PV module characteristics at different irradiance levels. Fig. 12 illustrates the dynamic behavior of the proposed PV interface system when the PV module is suddenly subjected to shading while the load is set at 40Ω. The PV emulator is controlled to operate at irradiance levels of 1000W/m^2, 750W/m^2, and 500W/m^2, simultaneously. The little decrease of v_{pv} with noticeable decrease of i_{pv}, when reducing irradiance level, indicates that the MPPT unit changes the operating point of the PV emulator to a new MPP corresponding to the shading condition. In addition, the proposed system increases d_b to transfer more power from the battery port as a supplement to

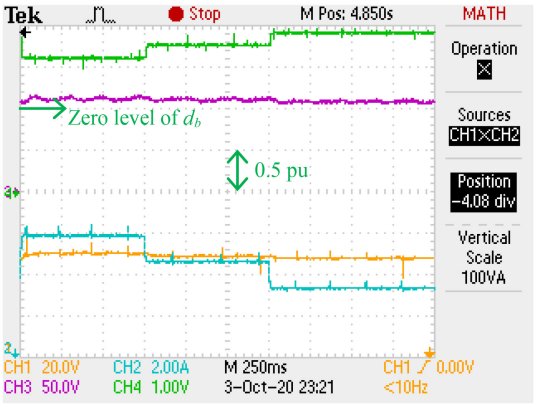

FIGURE 12. Performance at PV shading: CH1=v_{pv}, CH2=i_{pv}, CH3=v_o, and CH4= d_b.

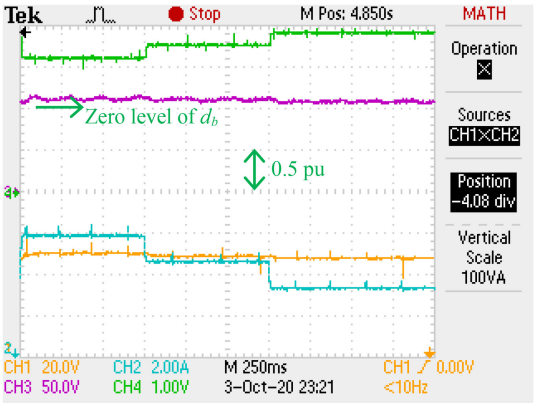

FIGURE 13. Performance at load change: CH1= v_o, CH2= i_o, CH4= d_b.

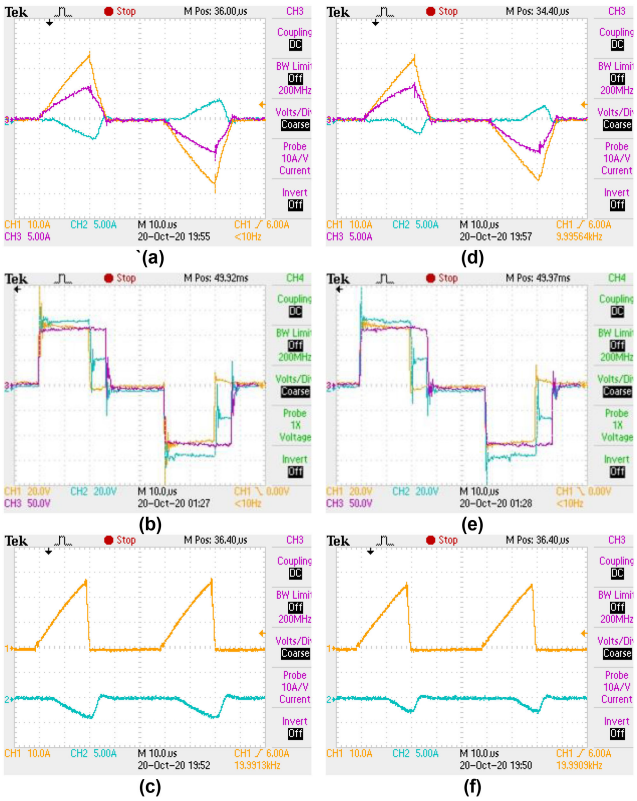

FIGURE 14. Battery charging during load change: (a), (b) The windings currents: CH1=i_{1pv}, CH2=i_{1b}, CH3= i_r, (c), (d) The windings voltage: CH1=v_{1pv}, CH2=v_{1b}, CH3= v_r, and (e), (f) The input ports currents: CH1=i_{ipv}, CH2=i_{ib}.

the decrease in PV power. Consequently, the proposed system succeeds to tightly regulating the load voltage v_o while the PV power is varying due to the shading condition.

The dynamic performance of the proposed system under load change is demonstrated in Fig. 13. In this test scenario, the PV emulator is set to feed 300W. The load voltage is tightly regulated under suddenly variation of the load resistance from 60Ω to 50Ω to 40Ω. Correspondingly, the load current i_o is increasing. During the first and second load settings, d_b is negative which indicates that the battery port is absorbing power from the PV port to keep the load voltage at the desired level. At the final load increase, d_b is reversed smoothly to positive value and both ports feed the load. It is obvious that the dynamic behavior of the experimental prototype coincides with the simulation results of Figs. 8 and 9. The proposed system succeeds to harvest the maximum power from the PV module while regulating the load voltage by controlling the duty ratios of the TPC.

The transformer voltages and currents during battery charging of the proposed TPC, which are analyzed in Fig. 5, are verified in Fig. 14. Fig. 14(a), (b), and (c) illustrate the windings currents, voltages, and the input ports currents, respectively, at 60Ω load resistance. When the load resistance is decreased while the PV emulator is set at the same operating point, the windings currents, voltages, and the input ports currents are shown in Fig. 14(d), (e), and (f), respectively. The five modes of operations during battery charging, analyzed in Section IV, are recognized in both cases of Fig. 14. In addition, it can be observed that increasing the load power cause the controller of the proposed TPC to reduce d_b to lessen the power transfer to the battery port in order to keep the load voltage level. Moreover, the battery port current i_{ib} is the rectified version of i_{1b}, whereas the decaying parts of the i_{1pv} disappear from the waveform of the PV port current i_{ipv}. This action should be expected as once the PV port inverter is switched to the zero-state, the stored energy in the leakage inductances of the transformer is freewheeling though switches of the PV port inverter to charge the battery pack and to feed the output port, as discussed in Subsection IV.C.

The windings currents, voltages, and input ports currents, during battery discharging operation of the proposed TPC, are demonstrated in Fig. 15(a), (b), (c) and Fig. 15(d), (e), (f) when the irradiance reference signal for the PV emulator is changed from 750 W/m^2 to 250W/m^2, respectively, at rated load condition. The five modes of operations during battery discharging, discussed in Section V, are distinguished in both cases of Fig. 15. Moreover, it is clear that reducing the irradiance level and hence the available PV power

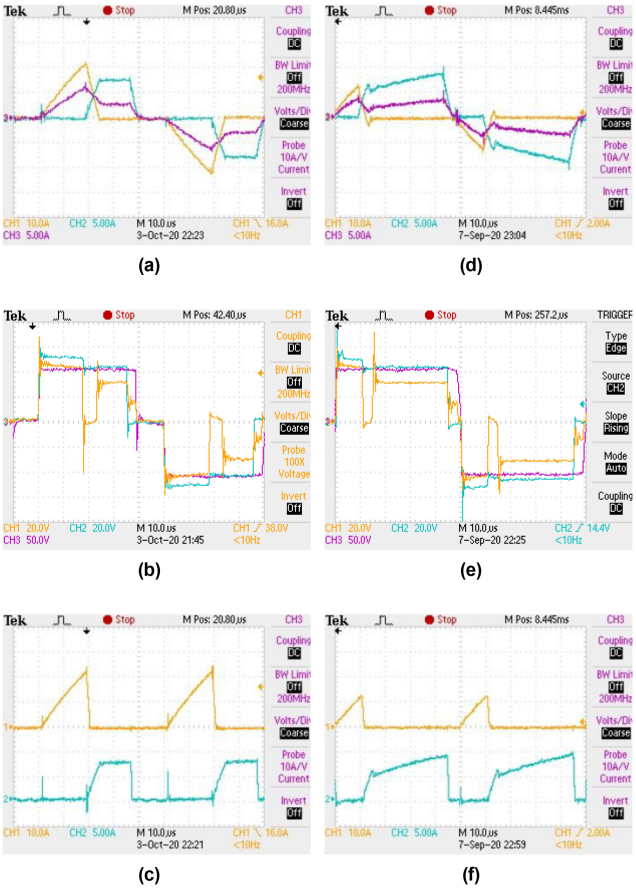

FIGURE 15. **Battery discharging at PV shading: (a), (b) The windings currents: CH1=i_{1pv}, CH2=i_{1b}, CH3= i_r, (c), (d) The windings voltage: CH1=v_{1pv}, CH2=v_{1b}, CH3= v_r, and (e), (f) The input ports currents: CH1=i_{ipv}, CH2=i_{ib}.**

renders the MPPT to reduce d_{pv}. Consequently, the voltage regulation loop of the proposed TPC increases d_b to boost the power transfer from the battery port in order to keep the load voltage at the desired level. It is worth mentioned that the decaying parts of i_{1b} and i_{1pv} are not feedback to their corresponding power sources as per discussions of modes 2 and 4, respectively, during battery discharging operation in Section V. The efficiency of the proposed converter is varying with the loading condition from 89.5% to 95.4%. The efficiency range could be further improved if circuit components are optimized.

VII. CONCLUSION

This paper introduces a new TPC topology for integrated PV-battery system to feed an isolated load. The proposed TPC topology is based on using auxiliary switches connected to active bridge at each port of the TPC to insure zero circulating current flow between battery and PV ports. Another contribution presented in this article is the simple switching scheme based on pulse width modulation of the PV and battery ports to keep the load voltage at the desired setting. This action eliminates the disadvantages of the phase shift control technique which is used widely for TABs. Simulation results demonstrate precise MPPT and tight load voltage regulation with fast response of the proposed integrated PV-battery system. In addition, the estimated settings of the dynamic limiters of duty ratios for the PV and battery ports are verified. Moreover, experimental results are presented to validate the analyses of the proposed TPC based integrated PV-battery system under different modes during battery charging and discharging operations. Furthermore, capabilities of the proposed system to keep the load voltage under different disturbances are exhibited. Future work will be directed to extend the proposed TPC to multiport converter with many bidirectional power flow ports to allow interfacing different ESS with the PV system.

ACKNOWLEDGMENT

The authors would like to thank PAAET and the college of technological studies for their support under the project number TS-21-09.

REFERENCES

[1] H. Zhu, D. Zhang, B. Zhang, and Z. Zhou, "A nonisolated three-port DC–DC converter and three-domain control method for PV-battery power systems," *IEEE Trans. Ind. Electron.*, vol. 62, no. 8, pp. 4937–4947, Aug. 2015.

[2] Z. Qian, O. Abdel-Rahman, H. Al-Atrash, and I. Batarseh, "Modeling and control of three-port DC/DC converter interface for satellite applications," *IEEE Trans. Power Electron.*, vol. 25, no. 3, pp. 637–649, Mar. 2010.

[3] H. Zhu, D. Zhang, Q. Liu, and Z. Zhou, "Three-port DC/DC converter with all ports current ripple cancellation using integrated magnetic technique," *IEEE Trans. Power Electron.*, vol. 31, no. 3, pp. 2174–2186, Mar. 2016.

[4] R. Faraji, H. Farzanehfard, G. Kampitsis, M. Mattavelli, E. Matioli, and M. Esteki, "Fully soft-switched high step-up nonisolated three-port DC–DC converter using GaN HEMTs," *IEEE Trans. Ind. Electron.*, vol. 67, no. 10, pp. 8371–8380, Oct. 2020.

[5] Z. Saadatizadeh, E. Babaei, F. Blaabjerg, and C. Cecati, "Three-port high step-up and high step-down DC-DC converter with zero input current ripple," *IEEE Trans. Power Electron.*, vol. 36, no. 2, pp. 1804–1813, Feb. 2021.

[6] J. Hong, J. Yin, Y. Liu, J. Peng, and H. Jiang, "Energy management and control strategy of photovoltaic/battery hybrid distributed power generation systems with an integrated three-port power converter," *IEEE Access*, vol. 7, pp. 82838–82847, 2019.

[7] X. Sun, Y. Shen, W. Li, and H. Wu, "A PWM and PFM hybrid modulated three-port converter for a standalone PV/battery power system," *IEEE J. Emerg. Sel. Topics Power Electron.*, vol. 3, no. 4, pp. 984–1000, Dec. 2015.

[8] J. Zeng, W. Qiao, and L. Qu, "An isolated three-port bidirectional DC–DC converter for photovoltaic systems with energy storage," *IEEE Trans. Ind. Appl.*, vol. 51, no. 4, pp. 3493–3503, Jul./Aug. 2015.

[9] H. Zhu, D. Zhang, H. S. Athab, B. Wu, and Y. Gu, "PV isolated three-port converter and energy-balancing control method for PV-battery power supply applications," *IEEE Trans. Ind. Electron.*, vol. 62, no. 6, pp. 3595–3606, Jun. 2015.

[10] L. P.-Botalla, G. G. Oggier, and G. O. García, "Extending the power transfer capability of a three-port DC–DC converter for hybrid energy storage systems," *IET Power Electron.*, vol. 10, no. 13, pp. 1687–1697, 2017.

[11] Z. Wang, Q. Luo, Y. Wei, D. Mou, X. Lu, and P. Sun, "Topology analysis and review of three-port DC–DC converter," *IEEE Trans. Power Electron.*, vol. 35, no. 11, pp. 11783–11800, Nov. 2020.

[12] I. Biswas, D. Kastha, and P. Bajpai, "Small signal modeling and decoupled controller design for a triple active bridge multiport DC–DC converter," *IEEE Trans. Power Electron.*, vol. 36, no. 2, pp. 1856–1869, Feb. 2021.
[13] B. Alajmi, I. M. Marei, I. Abdelsalam, and M. F. Alhajri, "Analysis and design of a multi-port DC-DC converter for interfacing PV systems," *Energies*, vol. 14, no. 7, 2021, Art. no. 1943, doi: 10.3390/en14071943.
[14] T. LaBella and J. Lai, "A hybrid resonant converter utilizing a bidirectional GaN AC switch for high-efficiency PV applications," *IEEE Trans. Ind. Appl.*, vol. 50, no. 5, pp. 3468–3475, Sep./Oct. 2014.
[15] D. Gunasekaran and L. Umanand, "Integrated magnetics based multiport bidirectional DC–DC converter topology for discontinuous-mode operation," *IET Power Electron.,* vol. 5, no. 7, pp. 935–944, 2012.
[16] M. Phattanasak, R. Gavagsaz-Ghoachani, J.-P. Martin, B. Nahid-Mobarakeh, S. Pierfederici, and B. Davat, "Control of a hybrid energy source comprising a fuel cell and two storage devices using isolated three-port bidirectional DC–DC converters," *IEEE Trans. Ind. Appl.*, vol. 51, no. 1, pp. 491–497, Jan./Feb. 2015.
[17] J.-Y. Lee and J.-H. Jung, "Modified three-port DAB converter employing voltage balancing capability for bipolar DC distribution system," *IEEE Trans. Ind. Electron.*, vol. 69, no. 7, pp. 6710–6721, Jul. 2022.
[18] V. Nair, S. Gulur, R. Chattopadhyay, and S Bhattacharya, "Integrating photovoltaics and battery energy storage to grid using triple active bridge and voltage source converters," in *Proc. IEEE-IECON*, Singapore, 2020, pp. 3691–3696.
[19] V.-L. Pham and K. Wada, "Applications of triple active bridge converter for future grid and integrated energy systems," *Energies,* vol. 13, no. 7, 2020, Art. no. 1577, doi: 10.3390/en13071577.
[20] M. Jafari, Z. Malekjamshidi, D. D. Lu, and J. Zhu, "Development of a fuzzy-logic-based energy management system for a multiport multioperation mode residential smart microgrid," *IEEE Trans. Power Electron.*, vol. 34, no. 4, pp. 3283–3301, Apr. 2019.
[21] H. M. El-Helw, M. Al-Hasheem, and M. I. Marei, "Control strategies for the DAB based PV interface system," *PLoS One*, vol. 11, no. 8, Aug. 2016, Art. no. e0161856.
[22] N. Noroozi, A. Emadi, and M. Narimani, "Performance evaluation of modulation techniques in single-phase dual active bridge converters," *IEEE Open J. Ind. Electron. Soc.*, vol. 2, pp. 410–427, 2021.
[23] S. Shao, X. Wu, J. Zhang, K. Sheng, and H. Chen, "Circulating current and ZVS-on of a dual active bridge DC-DC converter: A review," *IEEE Access*, vol. 7, pp. 50561–50572, 2019.
[24] V. N. S. R. Jakka, A. Shukla, and G. D. Demetriades, "Dual-transformer-based asymmetrical triple-port active bridge (DT-ATAB) isolated DC–DC converter," *IEEE Trans. Ind. Electron.*, vol. 64, no. 6, pp. 4549–4560, Jun. 2017.
[25] B. N. Alajmi, M. I. Marei, and I. Abdelsalam, "A multi-port DC/DC converter based on two- quadrant inverter topology for PV systems," *IEEE Trans. Power Electron.*, vol. 36, no. 1, pp. 522–532, Jan. 2021.
[26] M. I. Marei, B. Alajmi, I. Abdelsalam, and M. F. Alhajri, "A PV interface system based on high-gain high-frequency link converter," in *Proc. IEEE Universities Power Eng. Conf.*, Glasgow, U.K., Sep. 2018, pp. 1–6.
[27] M. Killi and S. Samanta, "Modified perturb and observe MPPT algorithm for drift avoidance in photovoltaic systems," *IEEE Trans. Ind. Electron.*, vol. 62, no. 9, pp. 5549–5559, Sep. 2015.

MOSTAFA I. MAREI (Senior Member, IEEE) received the B.Sc. (Hons.) and M.Sc. degrees in electrical engineering from Ain Shams University, Cairo, Egypt, in 1997 and 2000, respectively, and the Ph.D. degree in electrical engineering from the University of Waterloo, Waterloo, ON, Canada, in 2004.

From 2004 to 2006, he was a Postdoctoral Fellow with the University of Waterloo. He is currently a Professor with the Department of Electrical Power and Machines, Ain Shams University. His research interests include power electronics, distributed and renewable generation, microgrids, power quality, custom power, electrical drives, and artificial intelligent applications in power systems.

Prof. Marei was the recipient of Egypt State Incentive Award in Engineering Sciences 2013, NSERC Fellowship 2004–2006, Ontario Graduate Scholarship 2002–2003. His biography is listed in Marque's Who is Who in the World.

BADER N. ALAJMI (Senior Member, IEEE) received the B.Sc. and M.Sc. degrees from California State University, Fresno, CA, USA, in 2001 and 2006, respectively, and the Ph.D. degree in power electronics from the University of Strathclyde, Glasgow, U.K., in 2013. He is currently an Assistant Professor with the College of Technological Studies, Public Authority of Applied Education and Training, Adiliya, Kuwait. His research interests include digital control of power electronic systems, microgrids and distributed generation, and renewable energy.

IBRAHIM ABDELSALAM (Senior Member, IEEE) received a B.Sc. (with first-class) and M.Sc. degrees in electrical engineering from the Arab Academy for Science and Technology and Maritime Transport, Alexandria, Egypt, in 2006 and 2009, respectively, and the Ph.D. degree in power electronics from the University of Strathclyde, Glasgow, U.K., in 2016. He is currently an Associate Professor with Electrical Department, Arab Academy for Science and Technology and Maritime Transport. His research interests include power electronic converters and their applications in wind energy conversion systems, and advanced control strategies of the multilevel voltage and current source converters.

NABIL A. AHMED (Senior Member, IEEE) received the B.Sc. and M.Sc. degrees in electrical engineering from the Electrical and Electronics Engineering Department, Assiut University, Asyut, Egypt, and the Ph.D. degree in electrical engineering from the University of Toyama, Toyama, Japan, in 1989, 1994, and 2000, respectively.

Since 1989, he has been with Assiut University, where he has been a Professor since 2011. He was a Postdoctoral Fellow with the Electrical Engineering Saving Research Center, Kyungnam University, Changwon, South Korea, from October 2004 to April 2005, and a JSPS Post Doctorate Fellow with Sophia University, Tokyo, Japan from July 2005 to September 2006. He is currently an Associate Professor with the Electrical Engineering Department, College of Technological Studies, Public Authority of Applied Education and Training, Kuwait, on leave from Assiut University. His research interests include power electronics applications, variable speed drives, soft switching converters, renewable energy systems, and its integration to electric power grid.

Prof. Ahmed was the recipient of Egypt State Encouraging of Research Prize 2005, Japan Monbusho Scholarship 1996–2000, JSPS Fellowship 2005–2007, Best Paper Awards from ICEMS'05 and IATC'06 conferences and Best Presentation Award from ICEMS'04 conference. He has been listed in Marque's Who is Who in the World since 2009. Prof. Ahmed is a Member of the IEEE Industrial Electronics Society.